ARTICLE OPEN

Check for updates

Winter heavy precipitation events over Northern Europe modulated by a weaker NAO variability by the end of the 21st century

Ramón Fuentes-Franco [1,2 ✉], David Docquier [3], Torben Koenigk[1,2], Klaus Zimmermann [1,2] and Filippo Giorgi[4]

We use an ensemble of models participating in the Coupled Model Intercomparison Project phase 6 (CMIP6) to analyse the number of days with extreme winter precipitation over Northern Europe and its relationship to the North Atlantic Oscillation (NAO), for the historical period 1950–2014 and two future 21st-century scenarios. Here we find that over Northern Europe, the models project twice more extreme precipitation days by the end of the 21st century under the high-emission scenario compared to the historical period. We also find a weakening of the NAO variability in the second half of the 21st century in the high greenhouse gas emission scenario compared to the historical period, as well as an increasing correlation between extreme winter precipitation events and the NAO index in both future scenarios. Models with a projected decrease in the NAO variability across the 21st century show a positive trend in the number of days with extreme winter precipitation over Northern Europe. These results highlight the role played by NAO in modulating extreme winter precipitation events.

INTRODUCTION

An exponential increase in the water-holding capacity of the atmosphere is expected to happen as a consequence of temperature increase, current observations have shown the behaviour from the theoretical expectation[1–4]. One of the effects of global warming is that the risk of extreme precipitation events increases substantially. The frequency and intensity of heavy precipitation events have increased since the 1950s over most land areas where data coverage is sufficient, and they will continue to become more frequent and intensify in a warmer world[5–7]. In Europe, despite different regional trends in mean precipitation (positive in the North and negative in the South[8,]), extreme precipitation events show a general tendency to increase over the recent past and according to future model projections[6,9–12]. Climate-related extremes caused economic losses amounting to EUR 487 billion in the European Economic Area within the 1980–2020 period, which accounted for 80% of total economic losses caused by natural hazards according to the European Environment Agency (https://www.eea.europa.eu/ims/economic-losses-from-climate-related). Furthermore, besides changes in the frequency and severity of weather events, the future cost of climate-related hazards depends also on the size of the populations and the value of the assets exposed.

Precipitation and temperature variability over large parts of Europe and Greenland are modulated by the North Atlantic Oscillation (NAO)[13,14], defined as the mean sea-level pressure (SLP) difference between the Subtropical High over the Azores and the Subpolar Low over Iceland (Methods). The positive (negative) NAO phase occurs when this gradient is increased (decreased), which causes a northward (southward) shift in the atmospheric jet stream, increased mid-latitude westerly winds, and increased storminess in the northern (southern) part of the North Atlantic Ocean, hence causing warmer and wetter conditions than normal

in Northern (Southern) Europe, and drier and colder than normal conditions in Southern (Northern) Europe[15].

Observational studies have also shown that the NAO has a strong influence on extreme winter precipitation, with a significant positive correlation in Northern and Western Europe, and a negative correlation over Southern Europe, thus creating a dipole-type pattern of extreme winter precipitation anomaly[9,12,16].

Due to the strong link between the NAO and extreme winter precipitation, climate model predictions and projections of the NAO are key for estimating extreme winter precipitation in Europe in the upcoming seasons and decades. It has been recently shown that the winter NAO and its effects on European climate are highly predictable on decadal timescales when using large ensembles of newly developed decadal prediction experiments[17,18] or decadal hindcasts from the coupled model intercomparison project (CMIP) phases 5 and 6[15].

The predictable atmospheric anomalies represent a forced response to oceanic low-frequency variability that strongly resembles the Atlantic multi-decadal variability (AMV)[19,20], correctly reproduced in the decadal hindcasts thanks to realistic ocean initialisation and ocean dynamics[17].

In this study, we analyse historical model simulations and future projections of the NAO and its relationship with extreme winter precipitation in Europe from the last generation of coupled global climate models participating in the CMIP6 intercomparison[21]. Future model projections follow the Shared Socioeconomic Pathways (SSP[22]) based on a low emission scenario reaching 2.6 W/m^2 (SSP1–2.6) and a high emission scenario reaching 8.5 W/m^2 (SSP5–8.5) by 2100. We use 42 models (Supplementary Table 1), each with several ensemble members to distinguish the trends in extreme winter precipitation from internal variability. Our study aims to investigate the relationship between the NAO and extreme winter precipitation events in Europe over the historical period (1950–2014) and the 21st century (2015–2100).

[1]Rossby Centre, Swedish Meteorological and Hydrological Institute, Norrköping, Sweden. [2]Bolin Centre for Climate Research, Stockholm University, Stockholm, Sweden. [3]Royal Meteorological Institute of Belgium, Brussels, Belgium. [4]International Centre for Theoretical Physics, Trieste, Italy. ✉email: ramon.fuentesfranco@smhi.se
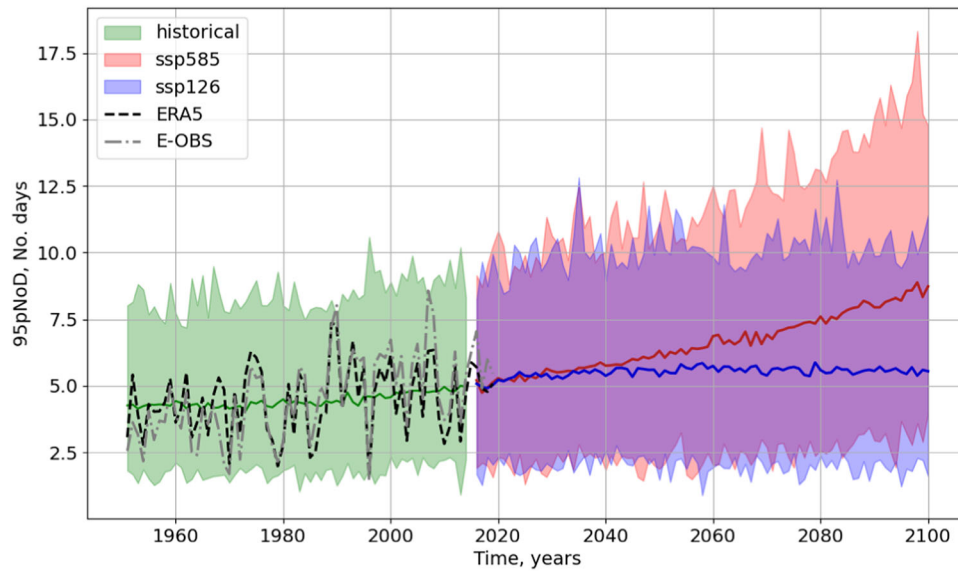
Fig. 1   Time series of 95pNoD for Northern Europe (57.8°N–71°N, 2.7°E–35°E). The ERA5 data are shown with a black dotted line. The coloured shaded area shows the range (minimum and maximum) of CMIP6 models in the historical (green) and 21st-century projections following SSP1–2.6 (blue) and SSP5–8.5 (red). The CMIP6 ensemble mean is shown with solid green (historical), blue (SSP1–2.6) and red (SSP5–8.5) lines. Every year in the 21st century had a statistically significant ($p < 0.05$) higher mean than the historical mean in both SSPs.

RESULTS

Extreme precipitation in future projections

The spatial patterns of the 95th percentile of daily precipitation (P95) over the winter season (December to February) from ERA5 and CMIP6 ensemble show high similarity to E-OBS (Supplementary Fig. 1). Over Northern Europe (Norway, Sweden, Denmark and Finland), the maximum P95 values vary regionally, from 31 mm per day as the overall maximum in the southern Norwegian coast to 15 mm per day in the southwestern tip of Sweden, 9 mm per day in Denmark and 8 mm per day in the south of Finland. Regional minimum P95 values are found over northern Finland and Sweden at 3.8 mm per day. Therefore the number of days exceeding the P95 values has a particular impact on Atlantic coastal areas.

In general, the average number of days with heavy precipitation, exceeding the 95th percentile (95pNoD) over the winter season, is 5% of 90 or 91 days, i.e. 4.5 days. Averaged over Northern Europe, the year-to-year variability of 95pNoD ranges from 2 to 8 days within the 1950–2019 period and has a positive trend of 27 min/year (or ~4.5 h per decade) in the ERA5 analysis and 69 min/year (11.5 h per decade) in E-OBS (Fig. 1). The range of CMIP6 models captures the interannual variability of ERA5 and E-OBS over the historical period (1950–2014), and the multi-model average shows a positive trend of 16 min/year (or ~2.6 h per decade), which is smaller than ERA5 and E-OBS but statistically significant ($p < 0.01$). The multi-model trend increases to 100 min/year (or 16.6 h/decade) ($p < 0.01$) in the last two decades of the 21st century following the SSP5–8.5. All years from the future projections have a statistically significant ($p < 0.05$) higher mean 95pNoD than the historical period. The SSP1–2.6 scenario shows a maximum in the middle of the 21st century, with a negative trend in the last decades of the 21st century, reaching a mean of >5 days per season by 2100, while the SSP5–8.5 scenario shows an increased trend by the end of the 21st century, reaching a mean of >8 days per season by 2100. This is particularly relevant for regions that already show high P95 values in the current climate since a projected mean 95pNoD larger than 8 days per season means that, e.g., Norwegian coastal areas are projected to have on average more than 240 mm of precipitation in eight days during the winter season under the SSP5–8.5 scenario.

The North Atlantic oscillation modulates extreme precipitation. In turn, for the NAO time series, the SSP1–2.6 scenario does not show a significant trend in the mean NAO value, although minimum values of NAO in several years during the 21st century are lower than in the historical period (Fig. 2a), which does not occur for SSP5–8.5 (Fig. 2b). Consequently, the ensemble mean NAO in SSP5–8.5 shows significantly higher values than in the historical period ($p < 0.05$). This is particularly noticeable in the last twenty years of the 21st century, showing 8 years with significantly higher NAO values than the historical period (Fig. 2b).

There is a significant correlation ($p < 0.01$) between the NAO and 95pNoD in Northern Europe according to ERA5 over 1979–2019 ($r = 0.61$). All CMIP6 models agree on the sign of the precipitation-NAO correlation (increase in precipitation with larger NAO values), but most of them underestimate this correlation when compared to ERA5 (ensemble mean r ~0.42; Fig. 3). For the future period, all models show a stronger precipitation-NAO correlation compared with the historical period (Fig. 3). While the historical period and the SSP1–2.6 scenarios do not show a significant correlation between the 95pNoD trend and the intensity of the NAO-95pNoD correlation, the SSP5–8.5 scenario shows a significant tendency toward a higher NAO-95pNoD correlation for models with a higher 95pNoD trend over Northern Europe ($r = 0.18$; $p < 0.01$; Fig. 3). Therefore, based on the CMIP6 projections, we find that under the high emission scenario, models that show a more pronounced trend in 95pNoD also show more sensitivity of 95pNoD to NAO variability. This suggests that as the number of days with extreme winter precipitation increases in Northern Europe, their dependency on NAO increases (as seen from the larger regression slope in Fig. 3).

Because of the strong link between NAO and precipitation, future changes in NAO variability impact the variability of extreme winter precipitation. NAO interannual variability (standard deviation computed over all years of the historical period) from ERA5 lies in the upper part of the CMIP6 ensemble with 8.97 hPa (Fig. 4a). For the SSP1–2.6 scenario, there is a non-significant increase in NAO variability in the last half of the 21st century compared to the historical period (Fig. 4b). For SSP5–8.5, although a stronger correlation between 95pNoD and NAO is found in the 21st century (Fig. 3c), CMIP6 models show a decrease in the NAO variability, from a mean standard deviation of 8.5 hPa in the
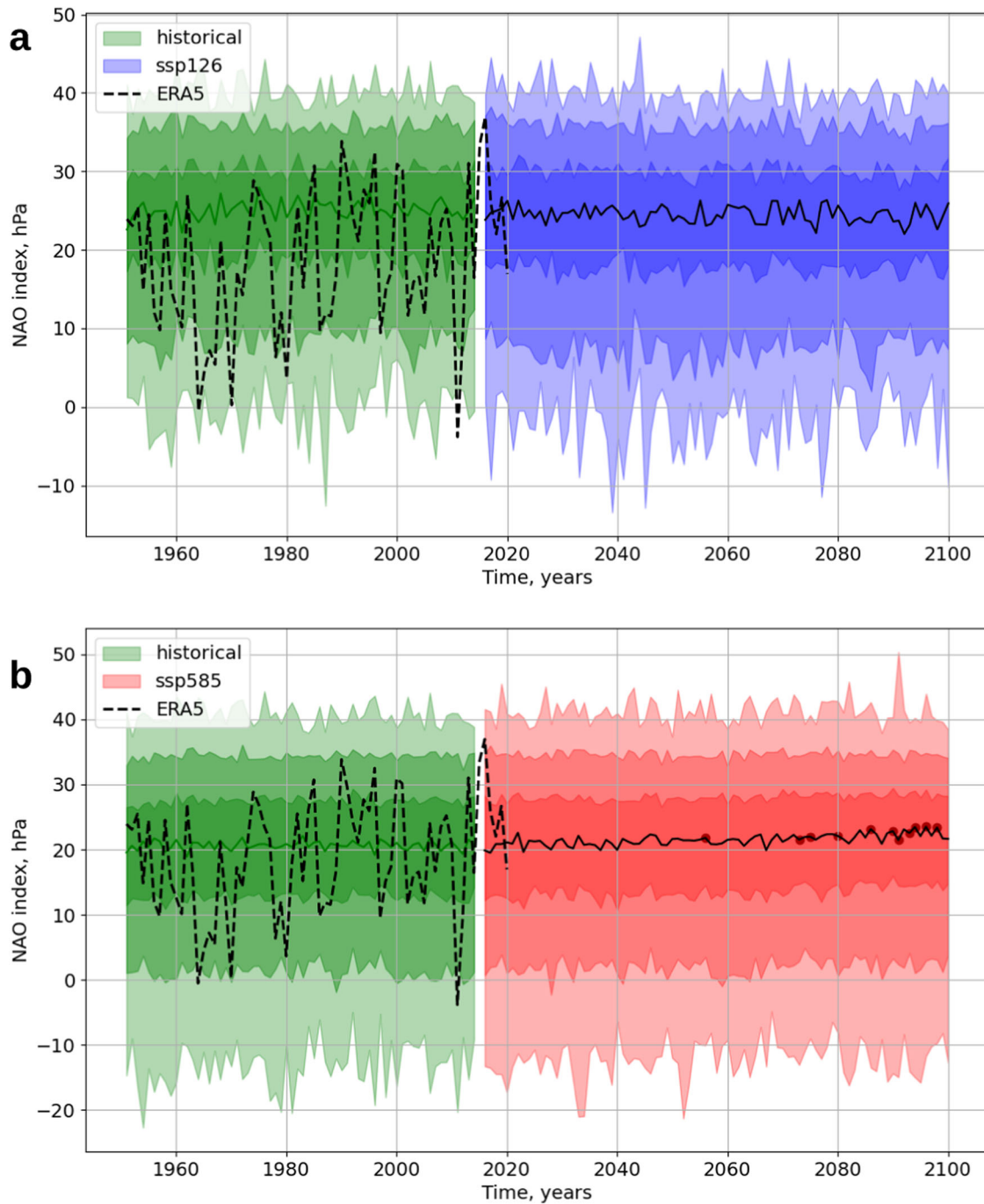
Fig. 2 Time series of NAO. ERA5 data are shown with a black dotted line. The coloured shaded area shows the range of CMIP6 models in the historical (green) and 21st-century projections following **a** SSP1–2.6 (blue) and **b** SSP5–8.5 (red). The CMIP6 ensemble mean is shown with solid green (historical) and black (SSPs) lines. For every year in the 21st century, a statistically significant ($p < 0.05$) higher mean than the historical mean is shown with a dark-red dot.

historical period to less than 7 hPa in the future (Fig. 4ct). Furthermore, for SSP5–8.5, the models with a smaller future NAO standard deviation show a greater 95pNoD trend. The relationship between the NAO standard deviation and 95pNoD trend in the future shows a significant ($p < 0.01$) correlation of $r = -0.18$ (Fig. 4c). This means that the higher trend in 95pNoD in Northern Europe in the future is associated with a lower NAO variability under the high greenhouse emission scenario. The weakening of the NAO standard deviation in the SSP5–8.5 scenario is due to less intense negative NAO phases (Fig. 2b) since there is a significant tendency of models with reduced standard deviation to show an

increase in the NAO-mean values (Supplementary Fig. 2a). This explains why models with reduced NAO standard deviation, and hence higher mean NAO values, show higher 95pNoD trends (Supplementary Fig. 2b).

In summary, although future model projections show a weakening of NAO variability (i.e. lower standard deviation) in SSP5–8.5 due to less intense negative NAO phases, the number of days with extreme winter precipitation increases in Northern Europe and is more correlated to NAO than in historical climatic conditions. While for the low emission scenario, model projections show no significant change in NAO variability, a positive but not
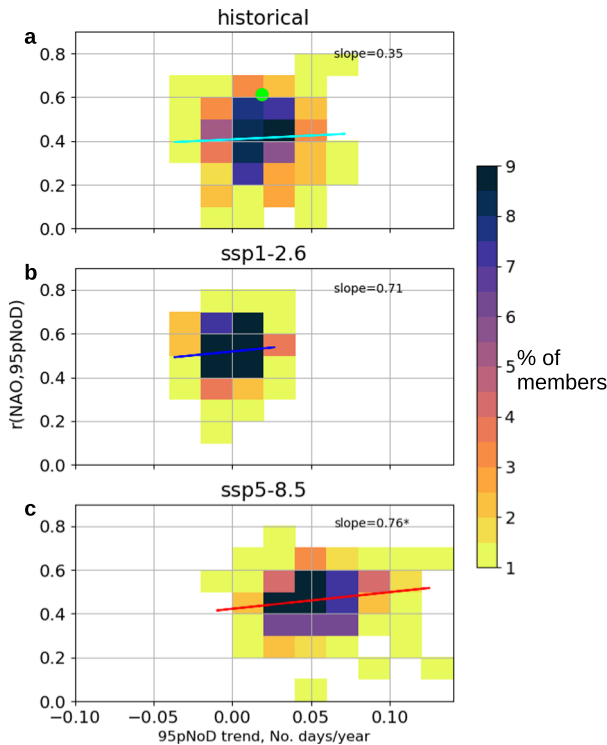
R. Fuentes-Franco et al.

Fig. 3 Relation between NAO-95pNoD correlation and 95pNoD trend. Two-dimensional histograms of the NAO-95pNoD correlation (r(NAO, 95pNoD)) against 95pNoD trend, for **a** the 1970–2014 period, the 2050–2099 period for **b** SSP1–2.6 and **c** SSP5–8.5. The colour bar shows the percentage of models within a bin. The linear regression of r(NAO, 95pNoD) onto the 95pNoD trend is shown with a line in every subplot, and the slope of the linear regression is provided in every subplot (an asterisk is present when the linear regression is significantly different from zero, $p < 0.05$). ERA5 data are shown with a green circle in the historical subplot (**a**).

Fig. 4 Relation between NAO's standard deviation and 95pNoD trend. Two-dimensional histograms of the NAO's standard deviation against 95pNoD trend for **a** the 1970–2014 period, the 2050–2099 period for **b** SSP1–2.6 and **c** SSP5–8.5. The colour bar shows the percentage of models within a bin. The linear regression of the NAO's standard deviation onto the 95pNoD trend is shown for the three subplots, and the slope of the linear regression is provided in every subplot (an asterisk is present when the linear regression is significantly different from zero, $p < 0.05$). ERA5 data are shown with a green circle in the historical subplot (**a**).

significant tendency to increase the 95pNoD trend with increased NAO standard deviation appears.

Compared to ERA5 (Fig. 5a), the modelled regression of NAO index onto SLP in both SSP1–2.6 and SSP5–8.5 shows an overestimation (~+0.50 hPa, <+0.25 hPa, respectively, Supplementary Fig. 5) of the intensity of the Icelandic low (it is core ~ −6 hPa in ERA5, Fig. 5a). The two scenarios also show an underestimation (>−0.40 hPa for both) of the Azores' high-SLP intensity which is ~3.5 hPa in ERA5. The regression of 95pNoD onto the NAO index in ERA5 shows positive values extending across the northernmost areas of the North Atlantic from eastern Greenland to the Fennoscandia peninsula and maxima over the Norwegian coast and the Norwegian Sea. Negative regression values extend from the east coast of the United States, over the subtropical North Atlantic Ocean towards Eastern Europe, with a minimum over the Iberian peninsula (Fig. 5b).

Although CMIP6 biases extend consistently across the North Atlantic and Europe (Supplementary Figs. 5 and 6) in both scenarios, the SSP5–8.5 scenario shows a smaller bias compared to SSP1–2.6. This is partly due to the larger number of ensemble members used in SSP5–8.5 compared to SSP1–2.6 (Supplementary Fig. 3). Our results are similar to previous works[23–25], where it has been reported that although CMIP6 models reduce the spatial bias of the NAO pattern, compared to CMIP3 and CMIP5 models, CMIP6 models still show systematic weaknesses in the intensity of both the Azores high and the Icelandic low. Complementing previous studies, here we also show that the intensity of the NAO bias compared to the ERA5 reanalysis varies according to the number of models included in the study.
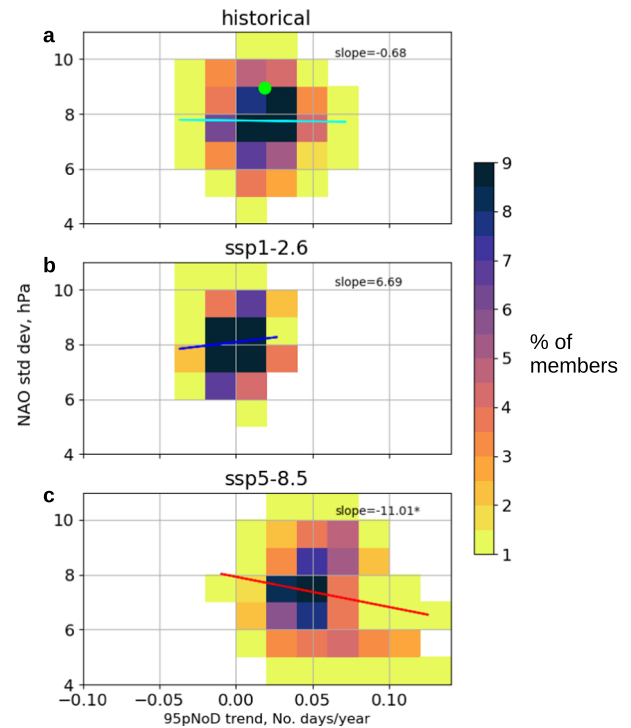
The regression of 95pNoD onto the NAO index in ERA5 shows values >1.5 days across all Nordic and Baltic countries, as well as the subpolar regions of the North Atlantic, while negative values < −2 days appear over the Iberian Peninsula and eastern Greenland (Fig. 5b). CMIP6 models underestimate the values found in ERA5 over Northern Europe (Supplementary Fig. 6).

The SLP spatial pattern in the future projections exhibit changes compared to the historical period when regressed onto the NAO-index (Fig. 5a, c, e). Consistent changes are found in both future scenarios, with increased SLP (up to 1 hPa) over the Barents Sea and the Nordic countries, and decreased SLP over the Labrador Sea (Fig. 5c, e). Models show a slightly weaker NAO in both future scenarios and a westward shift of the NAO pattern observed in historical simulations (Fig. 5c, e). In contrast to the NAO SLP pattern, and in line with previous results, the 95pNoD spatial pattern shows an intensification of the precipitation linked to NAO across the northernmost part of the North Atlantic and Northern Europe in both scenarios, with SSP5–8.5 showing a larger increase (Fig. 5d, f). The analysis of 95pNoD was carried out with models with different spatial resolutions with no interpolation carried out, except on the spatial patterns (Fig. 5d, f), in which interpolation to a common (relatively low) resolution grid (see Methods) was required. This interpolation to a common spatial resolution changes the intensity of the change due to coarsening of models with higher spatial resolution. The signal-to-noise ratio of the changes in SLP and 95pNoD (Fig. 6) shows that the areas with the strongest change, also show a signal-to-noise ratio greater than one, which means that the mean change across the model's ensemble is greater than the standard deviation of the change across the model's ensemble.
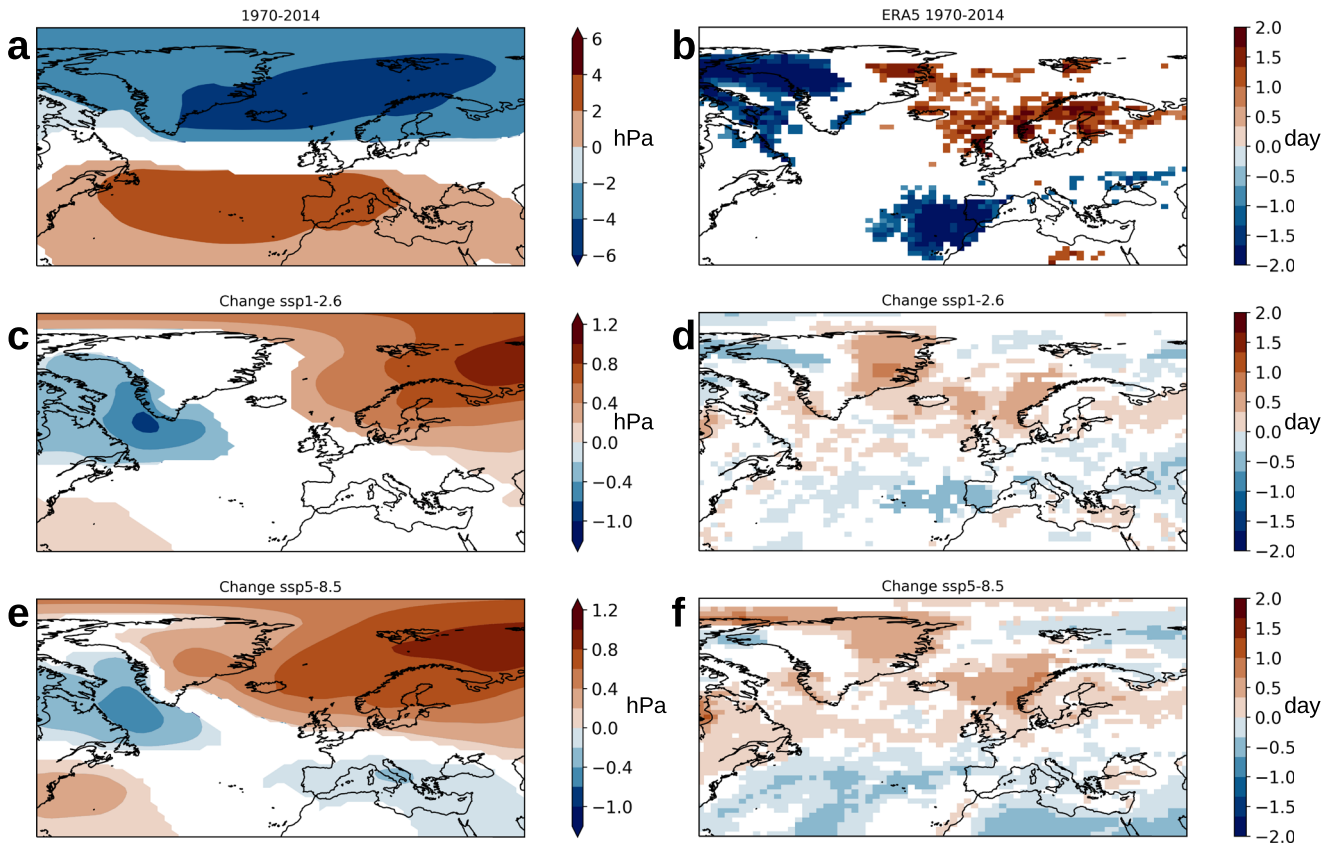
Fig. 5 Regression of SLP and 95pNoD onto the NAO index in the historical period, and their change by the end of the 21st century under the ssp1-2.6 and ssp5-8.5 scenarios. Regression of **a** SLP and **b** 95pNoD onto the standardised NAO index for ERA5. For CMIP6 models, the difference of the regression of SLP onto the standardised NAO index between the 2050–2099 period and the 1970–2014 period for **c** SSP1–2.6 and **e** SSP5–8.5. **d** and **f** similar to **c** and **e** for 95pNoD. Units are hPa for SLP and the number of days for 95pNoD. For 95pNoD, the regression was performed after detrending the NAO and 95pNoD data. The ensemble mean was calculated following the weighting described in the "Methods" section. The weights used for every model are shown in Supplementary Fig. 3. The schematic distribution of weights per ensemble member is shown in Supplementary Fig. 4.
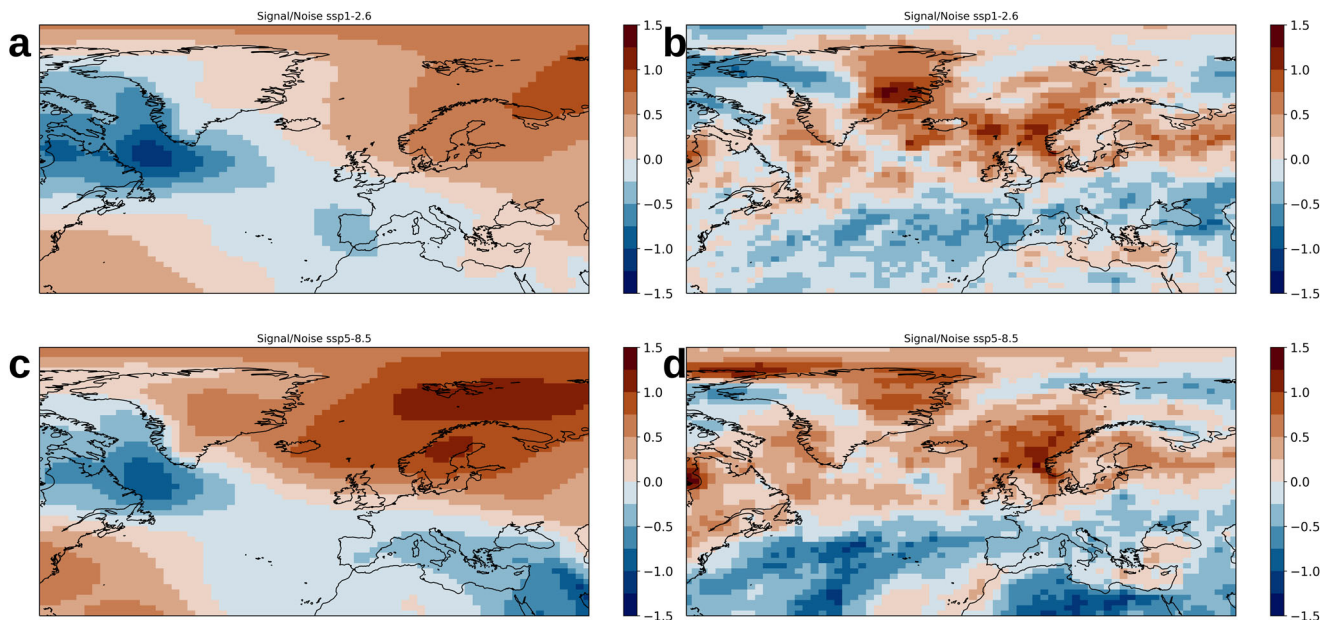

Fig. 6 Mean change divided by standard deviation of the change in SLP and precipitation. Ratio between mean sea level pressure change between 2050–2099 and 1970–2014 and standard deviation of the variability of sea level pressure change across ensemble members in SSP1–2.6 (**a**) and SSP5–8.5 (**c**). **b**, **d** similarly to (**a**) and (**c**), respectively for 95pNoD.

DISCUSSION

Projected changes in NAO depend on the models used. CMIP6 models show an underestimation of both the NAO variability (Supplementary Fig. 5, Fig. 4a) and its link to days with extreme precipitation (Fig. 3a, Supplementary Fig. 6). Models that are closer to ERA5 in simulating the NAO spatial pattern (lower mean squared error (MSE), Methods, Supplementary Fig. 7) and the NAO climatological intensity in the historical period ($NAO_{climhist}$, Methods, Supplementary Fig. 8) generally project a future weaker NAO.

In our analysis, we give a larger weight to models closer to ERA5 in terms of NAO (Methods). Noticeably, when we compute the ensemble means with the same weight given to every member, there is a larger departure from ERA5 than when using weights, especially in the SLP regression onto the NAO index (Supplementary Fig. 9a, b), and a slightly larger difference compared to ERA5 in the 95pNoD regression (Supplementary Fig. 9c, d).

Since CMIP6 models with a historically strong NAO (similar to ERA5) project a weaker future NAO, and conversely CMIP6 models with a historically weak NAO project a stronger future NAO, the same-weight-means show a smoother future change in SLP (Supplementary Fig. 10a, c). Interestingly, the changes in 95pNoD in both SSP scenarios with the same weight means (Supplementary Fig. 10b, d) show consistency and high similarity to the weighted means (Fig. 5d, f). Therefore, regardless of the SSP scenario, ensemble size, changes in NAO intensity, or the use of different weights for different ensemble members, CMIP6 models show consistency in the higher dependency of extreme precipitation on NAO (Fig. 5d, f, Supplementary Fig. 10b, d). This result provides further evidence that the SLP response to NAO only provides one perspective of the circulation, a result similar to McKenna and Maycock[26], who showed that the future response of wind speed (at 850 hPa) to NAO shows more congruent results across CMIP5/6 models over Europe than SLP.

CMIP6 models show good skill in representing the variability of the days exceeding the 95th percentile of daily precipitation during winter (see Fig. 1), and the spatial pattern of P95 compared to station-based observations (Supplementary Fig. 1). Although CMIP6 models tend to underestimate extreme precipitation events[27], they simulate extreme precipitation more strongly than CMIP5 and CMIP3[28], modelling factors have contributed to the stronger extreme precipitation, including the influences of higher spatial resolution and the improved model physics[29]. Although some models have increased their complexity in CMIP6 compared to CMIP5, models tend to reproduce precipitation extremes in a similar way as CMIP5[28,30]. Due to the heterogeneity of CMIP6 models, it is difficult to draw any firm conclusions on the impact of a specific process[31] which ultimately impacts the representation of days with extreme precipitation.

The increase in the trends of days with precipitation exceeding the 95th percentile of daily precipitation over Northern Europe is a robust feature found in CMIP5 and CMIP6 models. As the radiative forcing level increases the overall changing rate of the 95pNoD indicator increases[30]. Although model uncertainty and internal variability contribute to CMIP6 uncertainty on extreme precipitation, the intensification of extreme daily precipitation is robust over most regions of the planet, with more than 90% of models simulating an increase of 20-year return values[32].

A projected increase in the number of days with extreme winter precipitation impacting Northern Europe (Fig. 1), and its stronger linkage to the NAO (Figs. 3 and 5), make the NAO prediction increasingly relevant. Besides the evidence that the NAO phase and intensity can be predicted[15,17,18] mechanistically, the increased linkage between the NAO and ENSO, in future projections, has been reported to occur via both tropospheric and stratospheric pathways[33–37]. The stratospheric pathway starts with increased East Pacific rainfall due to warmer Pacific SST conditions caused by El Niño, which deepens the Aleutian Low. This drives the stratospheric

polar vortex southward, enhancing the negative phase of the NAO[38]. This process is reinforced by the tropospheric pathway in which the stronger Pacific subtropical jet extends into the Atlantic sector and more strongly influences the low-level winds in the Atlantic, contributing to amplifying the negative NAO phase[37]. Since El Niño-Southern Oscillation (ENSO) is the dominant interseasonal–interannual variability in the tropical Pacific and its impact extends globally, its predictability has been studied[39–42] and reaching lead times for up to 10 months[43]. The current climate NAO is modulated by ENSO (with El Niño inducing a negative NAO phase and La Niña a positive NAO phase[44]), increased dependence of NAO to ENSO, would increase NAO's predictability[37,45].

Most models analysed in this paper project a stronger negative correlation between NAO and ENSO in the second half of the 21st century compared to the historical period (Supplementary Fig. 11). This intensification of the NAO–ENSO relation (Supplementary Fig. 11), suggests that the NAO becomes more predictable in the future since ENSO has a higher predictability than NAO. However, there is a tendency in models with a stronger negative NAO–ENSO correlation to have a stronger NAO variability (Supplementary Fig. 11), this tendency existing in the historical period, becomes statistically significant ($p < 0.05$) in both future scenarios. As shown in Fig. 4, models with a stronger future NAO variability also show a lower 95pNoD trend under the high emission scenario, thus the higher NAO–ENSO correlation in the future would lead to a lower trend in 95pNoD in SSP5–8.5. Therefore, for models with a higher 95pNoD trend, due to their weak ENSO–NAO correlation in SSP5–8.5, ENSO would not provide more predictability to days with increasing extreme winter precipitation in the future. Instead, models that show a lower increase in 95pNoD show an enhanced linkage between ENSO, NAO and 95pNoD, making the relatively few extreme precipitation days more predictable.

Since the sea surface temperature anomaly (SSTA) response in the tropical North Atlantic (TNA) to ENSO and AMO are generally analogous, the TNA SSTA is an important means by which the AMO modulates the ENSO–NAO relationship[46]. The TNA SSTA causes strong NAO-like atmospheric circulation anomalies. When the AMO and ENSO are in phase, their influences on the TNA SSTA occur in superposition. Thus a strong TNA SSTA favours a significant NAO-associated atmospheric response, with El Niño (La Niña) and positive (negative) AMO causing a negative (positive) NAO phase. On the other hand, Zhang et al.[46] found that when AMO and ENSO are out of phase, the TNA SSTA responses counteract each other and thus the response of the NAO is very weak.

NAO has been associated with a tripole pattern in the North Atlantic SST, with negative SST anomalies in the Greenland and Irminger Seas to the Labrador Sea (Labrador here on) and positive SST anomalies in the central-western North Atlantic (subTNA) and again negative SST anomalies further south at the west African coast (Supplementary Fig. 12a)[47–49]. Most CMIP5 models have been found to reproduce the significant positive response in the subTNA near the American coast. However, in the subpolar region, the simulated locations and magnitude of the negative-response centres by most models differ from observations[50]. Here we find that for the end of the 21st century, CMIP6 models, project an intensified tripole pattern for the low-emission scenario (Supplementary Fig. 12b) and a weakened tripole pattern in the high-emission scenario, especially since the Labrador area changes towards a positive relationship with NAO when compared to the historical period (Supplementary Fig. 12c).

Here we find that CMIP6 models, in both historical and future projections, show that the more negative the trend in the difference between subTNA and Labrador SST (the less the difference between subTNA and Labrador SST), the lower the NAO variability (Fig. 7).

The ERA5 reanalysis shows that the relationship between surface temperature and the 95pNoDa has a similar NAO-surface temperature tripole pattern (Supplementary Fig. 13a) Models with a weaker NAO variability have both a weaker subpolar to subtropical SST
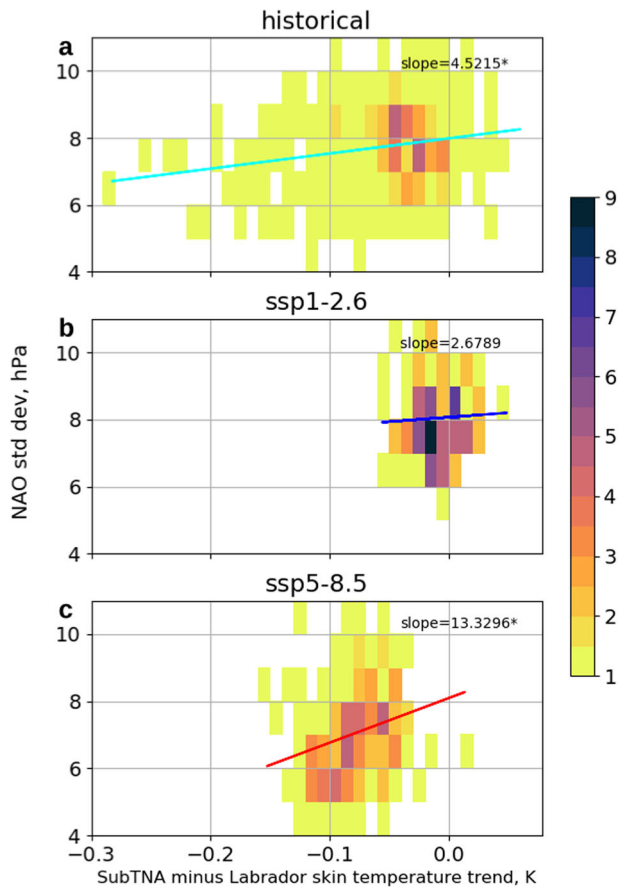
Fig. 7 Relation between the skin temperature difference between the subtropical North Atlantic (subTNA) and the Labrador Sea verus the NAO's standard deviation. Two-dimensional histogram of the skin temperature difference between the subtropical North Atlantic (subTNA) and the Labrador area versus the NAO's standard deviation for the **a** 1970–2014 period, the 2050–2099 period for **b** the ssp1–2.6 ensemble and **c** the SSP5–8.5 ensemble. Colour bar shows the percentage of models within a bin. The linear regression of both variables is shown for the three subplots. The slope of the linear regression is shown in every subplot, and it is marked with an asterisk when the linear regression is significantly different from zero ($p < 0.05$). ERA5 is shown with a green scatter point in the historical (**a**) subplot. The subTNA is calculated as the area average between the latitudes 30°N and 44°N and longitudes 80°W and 38°W. The Labrador Sea area was calculated as the area average of the skin temperature within latitudes 50°W and 77°W and longitudes 83°W and 30°W. Land points were masked out.

Fig. 8 Relation between the skin temperature in the Labrador Sea area versus 95pNoD. Two-dimensional histogram of the skin temperature in the Labrador Sea area versus 95pNoD for **a** the 1970–2014 period, the 2050–2099 period for the **b** the SSP1–2.6 ensemble and **c** the SSP5–8.5 ensemble. Colorbar shows the percentage of models within a bin. The linear regression of both variables is shown for the three subplots. The slope of the linear regression is shown in every subplot, and it is marked with an asterisk when the linear regression is significantly different from zero ($p < 0.05$).

gradient and a higher trend on 95pNoD under SSP5–8.5 (see Fig. 4). Colder SST in the Labrador area is associated with positive NAO[51], and hence with an increased number of extreme winter precipitation days in Northern Europe. Models reproduce this relationship in the historical and future SSP1–2.6 scenarios. In contrast, for the SSP5–8.5 scenario, a warmer than normal SST on the Labrador Sea still shows an increased 95pNoD (Fig. 8). Without removing the trends in both surface temperature and 95pNoD over Nordic countries, spatial changes in their relationship show that a more intense negative link between the surface temperature on the Labrador area and 95pNoD in the future under the SSP1–2.6 scenarios (Supplementary Fig. 13b), while a change towards 95pNoD being more positively related with the surface temperature in the whole North Atlantic, especially over the Arctic Ocean ($\Delta r > 0.4$, Supplementary Fig. 13d). When the trends in both the 95pNoD over the Nordic countries and the surface temperature are removed, the relationship change in the SSP1–2.6 scenario
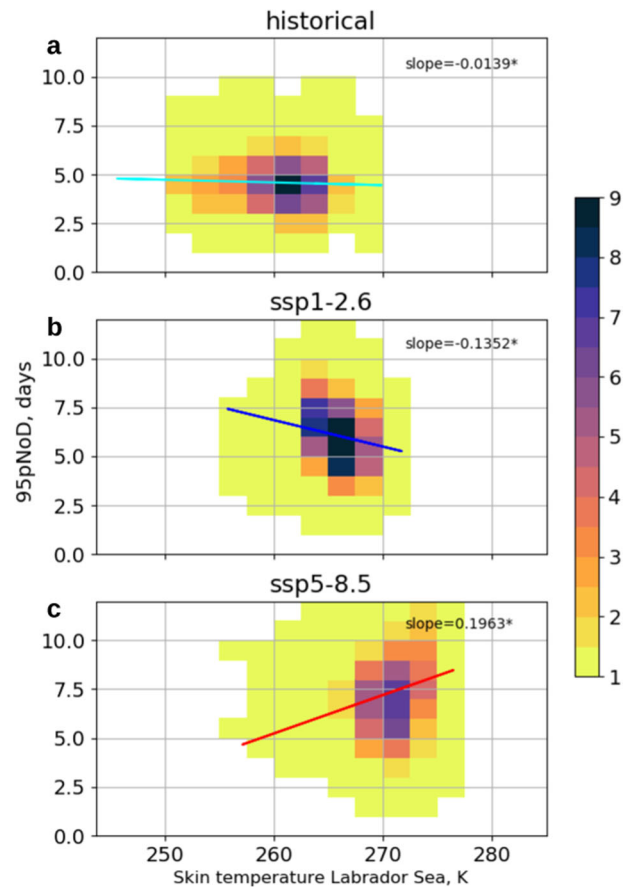
(Supplementary Fig. 13c) shows an alike spatial pattern as when trends are not removed. In contrast, the SSP5–8.5 scenario shows a similar pattern to SSP1–2.6. (Supplementary Fig. 13e). Therefore although we show that a warmer Arctic and North Atlantic, specifically a warmer Labrador Sea is linked to an increased 95pNoD (Fig. 8c), at interannual scales, a negative link between the surface temperature on the Labrador Sea is still projected to be related to 95pNoD variability.

In summary, a doubling in the number of days with extreme winter precipitation over Northern Europe is projected by CMIP6 models in the second half of the 21st century compared to the historical period (1950–2014). We show that model weighting based on how well models represent NAO does not change the results on the strengthening of the linkage between NAO and extreme precipitation over Northern Europe, making this a very consistent result among CMIP6 models, regardless of the biases representing NAO. Here we show that the number of days with extreme winter precipitation is strongly associated with the NAO in a warmer world, even though future projections show a weakening of this mode of variability, with a reduced Iceland–Azores sea level pressure gradient. This weakening of the NAO is due to less intense values during the negative phase of NAO, causing a shift of the climatological NAO mean towards higher values. We hypothesise

that this shift towards a more positive NAO is the reason for the increased relation with 95pNoD in Northern Europe.

The NAO in turn shows a stronger linkage to ENSO in future projections. However, models with a stronger future connection to ENSO also show a lower trend in the number of extreme winter precipitation days. Therefore, the higher dependency of NAO on ENSO would not necessarily imply that ENSO provides more predictability to days with extreme precipitation in the future. A warmer subpolar North Atlantic Ocean appears to play a role in the weakening of the Iceland-Azores surface pressure gradient; however, regardless of the weaker, more positive NAO, Northern European extreme winter precipitation appears to be more dependent on NAO, which might carry important consequences on its predictability.

METHODS

Data

Model data used in this study were obtained from the CMIP6 database[21]. The CMIP6 models used in this study and the number of ensemble members for SSP1–2.6 and SSP5–8.5 are provided in Supplementary Table 1. For all figures, and for every SSP, the same number of ensemble members were used during the historical period (1950–2014) and future projections (2015–2100). The future projections follow the SSP[22], 1 and 5 with a radiative forcing of 2.6 W/m^2 and 8.5 W/m^2 (SSP1–2.6 and SSP5–8.5, respectively). Different ensemble sizes for both SSPs were used due to the availability of simulations for every SSP by the time they were downloaded from the Earth System Gridded Federation (ESGF) nodes. We also use the European Centre for Medium-range Weather Forecasts (ECMWF) ERA5 reanalysis[52] over the period 1979–2020 at a spatial resolution of ~ 31 km. For precipitation, we also used the E-OBS dataset, a daily gridded land-only observational dataset covering the whole European continent. E-OBS station data come from the European National Meteorological and Hydrological Services.

Model weighting

For Fig. 5, different weights (*w*) were given to every ensemble member of all models depending on how similar the NAO pattern was compared to ERA5, through the calculation of the MSE of the regression of the NAO index onto the SLP (slpNAO). The MSE was calculated

$$MSE = \frac{1}{m} \sum_{j=0}^{m} (slpNAO_{ERA5} - slpNAO_i)^2 \qquad (1)$$

with *m* the total number of grid points within the latitudes 20°N and 90°N and longitudes 90°W and 60°E.

The calculation of the weights for every ensemble member *i* was based on a softmax function,

$$w(r)_i = \frac{e^{-r_i}}{\sum_{i=0}^{n} e^{-r_i}} \qquad (2)$$

where

$$r_i = k * (MSE_i - \min(MSE))/(\max(MSE) - \min(MSE))$$

with min(MSE) and max(MSE) being the minimum and maximum of the full ensemble, giving more weight to those ensemble members with lower MSE, and exponentially decreasing the weight as the MSE increases. The sum of all weights equals 1 by construction. *k* is a spread factor among weights, with a higher number providing a larger spread. In this case *k* = 100. The results using the model average (same weight for each member) can be found in Supplementary Fig. 8.

NAO, 95pNoD and ENSO definitions. The NAO index is defined as the difference in area-averaged SLP between the Azores (31.5°W–24.5°W, 36.5°N–40°N) and Iceland (25°W–13°W,

63°N–67°N)[37]. 95pNoD is defined as the number of days per season with precipitation larger than the 95th percentile of daily precipitation amount during the winter months (December to February). 95pNoD was calculated for both ERA5 and E-OBS data. The ENSO index is defined as the area-averaged Sea Surface Temperature (SST) in the Niño3.4 region, which is enclosed within the longitudes 170°W and 120°W, and the latitudes 5°S and 5°N. NAO and ENSO indices were calculated from monthly data.

Mean seasonal (December to February) data are used to calculate seasonal means for the NAO and ENSO indices. To produce the spatial patterns of NAO and 95pNoD (Fig. 5), all models were first interpolated to a 27,648-point (192 × 144) global longitude/latitude grid.

Pearson correlation between 95pNoD and NAO index, and between NAO and ENSO indices was calculated at a seasonal scale. Before performing the (Pearson) correlation analysis of Fig. 5b, d, f, the seasonal data of NAO, ENSO and 95pNoD were detrended.

The climatological NAO intensity used to produce Supplementary Fig. 6 and Supplementary Fig. 7, was calculated as the difference in the area-averaged SLP regressed onto the NAO index between the subtropical (31.5W–24.5°W,36.5°N–40°N) and subpolar (25°W–13°W, 63°N–67°N) regions.

REFERENCES

1. Trenberth, K. E., Dai, A., Rasmussen, R. M. & Parsons, D. B. The changing character of precipitation. *Bull. Am. Meteorol. Soc.* **84**, 1205–1217 (2003).
2. Pall, P., Allen, M. R. & Stone, D. A. Testing the Clausius-Clapeyron constraint on changes in extreme precipitation under CO2 warming. *Clim. Dyn.* **28**, 351–363 (2007).
3. Willett, K. M., Gillett, N. P., Jones, P. D. & Thorne, P. W. Attribution of observed surface humidity changes to human influence. *Nature* **449**, 710–712 (2007).
4. Min, S. K. et al. Human contribution to more-intense precipitation extremes. *Nature* **470**, 378–381 (2011).
5. IPCC. Summary for Policymakers. In: Climate Change 2021: The Physical Science Basis. Contribution of Working Group I to the Sixth Assessment Report of the Intergovernmental Panel on Climate Change (eds Masson-Delmotte, V. et al.). pp. 3–32 (Cambridge University Press, Cambridge, United Kingdom and New York, NY, USA, 2021).
6. Seneviratne, S. I. et al. (eds.). In *Climate Change 2021: The Physical Science Basis. Contribution of Working Group I to the Sixth Assessment Report of the Intergovernmental Panel on Climate Change*. 1513–1766 (Cambridge University Press, Cambridge, United Kingdom and New York, NY, USA, 2021).
7. Sun, Q., Zhang, X., Zwiers, F., Westra, S. & Alexander, L. V. *J. Clim.* **34**, 243–258 (2021).
8. Douville, H. et al. (eds.). In *Climate Change 2021: The Physical Science Basis. Contribution of Working Group I to the Sixth Assessment Report of the Intergovernmental Panel on Climate Change*. 1055–1210 (Cambridge University Press, Cambridge, United Kingdom and New York, NY, USA, 2021).
9. Cioffi, F., Lall, U., Rus, E. & Krishnamurthy, C. K. B. Space-time structure of extreme precipitation in Europe over the last century. *Int. J. Climatol.* **35**, 1749–1760 (2015).
10. Łupikasza, E. B. Seasonal patterns and consistency of extreme precipitation trends in Europe, December 1950 to February 2008. *Clim. Res.* **72**, 217–237 (2017).
11. Van den Besselaar, E. J. M., Klein Tank, A. M. G. & Buishand, T. A. Trends in European precipitation extremes over 1951–2010. *Int. J. Climatol.* **33**, 2682–2689 (2013).

12. Casanueva, A., Rodríguez-Puebla, C., Frías, M. D. & González-Reviriego, N. Variability of extreme precipitation over Europe and its relationships with teleconnection patterns. *Hydrol. Earth Syst. Sci.* **18**, 709–725 (2014).

13. Hurrell, J. W. Decadal trends in the North Atlantic Oscillation: Regional temperatures and precipitation. *Science* **269**, 676–679 (1995).

14. Delworth, T. L. et al. The North Atlantic Oscillation as a driver of rapid climate change in the Northern Hemisphere. *Nat. Geosci.* **9**, 509–512 (2016).

15. Smith, D. M. et al. North Atlantic climate far more predictable than models imply. *Nature* **583**, 796–800 (2020).

16. Tabari, H. & Willems, P. Lagged influence of Atlantic and Pacific climate patterns on European extreme precipitation. *Sci. Rep.* **8**, 5748 (2018).

17. Athanasiadis, P. J. et al. Decadal predictability of North Atlantic blocking and the NAO. *npj Clim. Atmos. Sci.* **3**, 20 (2020).

18. Klavans, J. M. et al. NAO predictability from external forcing in the late 20th century. *npj Clim. Atmos. Sci.* **4**, 22 (2021).

19. Häkkinen, S., Rhines, P. B. & Worthen, D. L. Atmospheric blocking and Atlantic multidecadal ocean variability. *Science* **334**, 655–659 (2011).

20. Frankignoul, C., Gastineau, G. & Kwon, Y. O. Wintertime atmospheric response to North Atlantic ocean circulation variability in a climate model. *J. Clim.* **28**, 7659–7677 (2015).

21. Eyring, V. et al. Overview of the Coupled Model Intercomparison Project Phase 6 (CMIP6) experimental design and organization. *Geosci. Model. Dev.* **9**, 1937–1958 (2016).

22. O'Neill, B. C. et al. The Scenario Model Intercomparison Project (ScenarioMIP) for CMIP6. *Geosci. Model. Dev.* **9**, 3461–3482 (2016).

23. Fasullo, J. T., Phillips, A. S. & Deser, C. Evaluation of leading modes of climate variability in the CMIP archives. *J. Clim.* **33**, 5527–5545 (2020).

24. Lee, J., Sperber, K. R., Gleckler, P. J., Taylor, K. E. & Bonfils, C. J. Benchmarking performance changes in the simulation of extratropical modes of variability across CMIP generations. *J. Clim.* **34**, 6945–6969 (2021).

25. Coburn, J. & Pryor, S. C. Differential credibility of climate modes in CMIP6. *J. Clim.* **34**, 8145–8164 (2021).

26. McKenna, C. M. & Maycock, A. C. Sources of uncertainty in multimodel large ensemble projections of the winter North Atlantic Oscillation. *Geophys. Res. Lett.* **48**, e2021GL093258 (2021).

27. Moreno-Chamarro, E., Caron, L. P., Ortega, P., Tomas, S. L. & Roberts, M. J. Can we trust CMIP5/6 future projections of European winter precipitation? *Environ. Res. Lett.* **16**, 054063 (2021).

28. Kim, Y. H., Min, S. K., Zhang, X., Sillmann, J. & Sandstad, M. Evaluation of the CMIP6 multi-model ensemble for climate extreme indices. *Weather Clim. Extremes* **29**, 100269 (2020).

29. Paik, S. et al. Determining the anthropogenic greenhouse gas contribution to the observed intensification of extreme precipitation. *Geophys. Res. Lett.* **47**, e2019GL086875 (2020).

30. Li, J., Huo, R., Chen, H., Zhao, Y. & Zhao, T. Comparative assessment and future prediction using CMIP6 and CMIP5 for annual precipitation and extreme precipitation simulation. *Front. Earth Sci.* **9**, 687976 (2021).

31. Séférian, R. et al. Tracking improvement in simulated marine biogeochemistry between CMIP5 and CMIP6. *Curr. Clim. Change Rep.* **6**, 95–119 (2020).

32. John, A., Douville, H., Ribes, A. & Yiou, P. Quantifying CMIP6 model uncertainties in extreme precipitation projections. *Weather Clim. Extremes* **36**, 100435 (2022).

33. Brönnimann, S. Impact of El Niño–southern oscillation on European climate. *Rev. Geophys.* **45**, RG3003 (2007).

34. Scaife, A. A. et al. Skillful long-range prediction of European and North American winters. *Geophys. Res. Lett.* **41**, 2514–2519 (2014).

35. Jiménez-Esteve, B. & Domeisen, D. I. The tropospheric pathway of the ENSO–North Atlantic teleconnection. *J. Clim.* **31**, 4563–4584 (2018).

36. Mezzina, B., García-Serrano, J., Bladé, I. & Kucharski, F. Dynamics of the ENSO teleconnection and NAO variability in the North Atlantic–European late winter. *J. Clim.* **33**, 907–923 (2020).

37. Fereday, D. R., Chadwick, R., Knight, J. R. & Scaife, A. A. Tropical rainfall linked to stronger future ENSO-NAO teleconnection in CMIP5 models. *Geophys. Res. Lett.* **47**, e2020GL088664 (2020).

38. Ineson, S. & Scaife, A. A. The role of the stratosphere in the European climate response to El Niño. *Nat. Geosci.* **2**, 32–36 (2009).

39. Latif, M. et al. A review of the predictability and prediction of ENSO. *J. Geophys. Res. Oceans* **103**, 14375–14393 (1998).

40. Barnston, A. G., Glantz, M. H. & He, Y. Predictive skill of statistical and dynamical climate models in SST forecasts during the 1997–98 El Niño Episode and the 1998 La Niña Onset. *Bull. Am. Meteorol. Soc.* **80**, 217–244 (1999).

41. Tang, Y. et al. Progress in ENSO prediction and predictability study. *Natl Sci. Rev.* **5**, 826–839 (2018).

42. Barnston, A. G., Tippett, M. K., L'Heureux, M. L., Li, S. & DeWitt, D. G. Skill of real-time seasonal ENSO model predictions during 2002–11: is our capability increasing? *Bull. Am. Meteorol. Soc.* **93**, 631–651 (2011).

43. Chen, H. C. et al. Enhancing the ENSO predictability beyond the spring barrier. *Sci. Rep.* **10**, 984 (2020).

44. Seager, R., Kushnir, Y., Nakamura, J., Ting, M. & Naik, N. Northern Hemisphere winter snow anomalies: ENSO, NAO and the winter of 2009/10. *Geophys. Res. Lett.* **37**, L14703 (2010).

45. Cassou, C. & Terray, L. Dual influence of Atlantic and Pacific SST anomalies on the North Atlantic/Europe winter climate. Geophysical research letters, 28(16), 3195-3198.C. Cassou, L. Terray, Dual influence of Atlantic and Pacific SST anomalies on the North Atlantic/Europe winter climate. *Geophys. Res. Lett.* **28**, 3195–3198 (2001).

46. Zhang, W., Mei, X., Geng, X., Turner, A. G. & Jin, F. F. A nonstationary ENSO–NAO relationship due to AMO modulation. *J. Clim.* **32**, 33–43 (2019).

47. Wanner, H. et al. North Atlantic Oscillation–concepts and studies. *Surv. Geophys.* **22**, 321–381 (2001).

48. Pinto, J. G. & Raible, C. C. Past and recent changes in the North Atlantic oscillation. WIRES. *Clim. Change* **3**, 79–90 (2012).

49. Årthun, M., Wills, R. C., Johnson, H. L., Chafik, L. & Langehaug, H. R. Mechanisms of decadal North Atlantic climate variability and implications for the recent cold anomaly. *J. Clim.* **34**, 3421–3439 (2021).

50. Jing, Y., Li, Y. & Xu, Y. Assessment of responses of North Atlantic winter sea surface temperature to the North Atlantic Oscillation on an interannual scale in 13 CMIP5 models. *Ocean Sci.* **16**, 1509–1527 (2020).

51. Robson, J., Ortega, P. & Sutton, R. A reversal of climatic trends in the North Atlantic since 2005. *Nat. Geosci.* **9**, 513–517 (2016).

52. Hersbach, H. et al. The ERA5 global reanalysis. *Q. J. R. Meteor. Soc.* **146**, 1999–2049 (2020).

ACKNOWLEDGEMENTS

AUTHOR CONTRIBUTIONS

R.F.F. led the work with contributions from D.D., T.K., K.Z. and F.G. R.F.F. performed the computations, analysed the results, produced the figures and led the paper writing. D.D., T.K., K.Z. and F.G. participated in the design of the study, the interpretation of the results and the writing of the paper.

COMPETING INTERESTS

The authors declare no competing interests.

ADDITIONAL INFORMATION

Supplementary information The online version contains supplementary material available at https://doi.org/10.1038/s41612-023-00396-1.

Correspondence and requests for materials should be addressed to Ramón Fuentes-Franco.

Reprints and permission information is available at http://www.nature.com/reprints

Publisher's note Springer Nature remains neutral with regard to jurisdictional claims in published maps and institutional affiliations.